Published in final edited form as:
J Am Chem Soc. 2009 March 11; 131(9): 3370–3376. doi:10.1021/ja809223s.

Identification of the Protonated Oxygenic Ligands of Ribonucleotide Reductase Intermediate X

Muralidharan Shanmugam[§], **Peter E. Doan**[§], **Nicholas S. Lees**, **JoAnne Stubbe**[‡,*], and **Brian M. Hoffman**[§,*]

[§] Department of Chemistry, Northwestern University, Evanston, IL, 60208-3113

[‡] Department of Chemistry, MIT, Cambridge, MA, 02139-4307

Abstract

We previously used a combination of CW and pulsed-ENDOR protocols to identify the types of protonated oxygen (OH_x) species and their disposition within the Fe^{III}/Fe^{IV} cluster of Intermediate **X**, the direct precursor of the essential diferric-tyrosyl radical cofactor of the $\beta 2$ subunit of *Escherichia coli* ribonucleotide reductase (RNR). We concluded that **X** contains the [(H_xO)$Fe^{III}OFe^{IV}$] fragment (**T** model), and does not contain a μ–hydroxo bridge. When combined with a subsequent ^{17}O ENDOR study of **X** prepared with $H_2{}^{17}O$ and with $^{17}O_2$, the results led us to suggest that this fragment is the entire inorganic core of **X**. This has been questioned by recent reports, but these reports do not themselves agree on the core of **X**. An experimental/computational study that included rapid freeze quench magnetic circular dichroism measurements and TD-DFT calculations [Mitic, N.; Clay, M. D.; Saleh, L.; Bollinger, J. M.; Solomon, E. I. *J. Am. Chem. Soc.* **2007**, *129*, 9049–9065] proposed that **X** has a μ-oxo/μ-hydroxo Fe^{III}/Fe^{IV} core, without addressing the existence of terminal (H_xO). In a series of computational studies, Noodleman and coworkers instead concluded that **X** possesses a di-μ–oxo Fe^{III}/Fe^{IV} core plus a terminal (H_2O) bound to Fe^{III} [eg., Han, W.-G.; Liu, T.; Lovell, T.; Noodleman, L. *J. Am. Chem. Soc.* **2005**, *127*, 15778–15790]. In this report we take advantage of improvements in 35 GHz pulsed-ENDOR performance to reexamine the protonation state of the oxygenic ligands of the inorganic core of **X** by directly probing the exchangeable proton(s) with ^2H pulsed-ENDOR spectroscopy. These ^2H ENDOR measurements confirm that **X** contains an Fe^{III}-bound terminal aqua ligand (H_xO), but the spectra contain *none* of the features that would be *required* for the proton of a bridging hydroxyl. Thus, we confirm that **X** contains a terminal aqua (plausibly hydroxo) ligand to Fe^{III} in addition to one or two μ–oxo bridges, but does not contain a μ–hydroxo bridge. The ^2H ENDOR measurements further demonstrate that this conclusion is applicable to both the WT and Y122F-$\beta 2$, and in fact detect no difference between the properties of protons on the terminal oxygens in the two variants; likewise, ^{14}N ENDOR measurements of histidyl ligands bound to Fe show no difference between the two variants.

Introduction

Diferrous non-heme iron proteins carry out a broad range of reactions, ranging from reversible O_2 binding to fatty acid desaturation and methane oxidation, and the factors that govern O_2 activation in such diverse reactions are of intense interest.[1–4] The $\beta 2$ (R2) subunit of class 1a and 1b *Escherichia coli* ribonucleotide reductases (RNR) are such proteins. These RNRs catalyze the conversion of nucleoside diphosphates to deoxynucleoside diphosphates in reactions involving complex free radical chemistry.[5–7] The $\beta 2$ subunits in their oxidized forms/

stubbe@MIT.EDU (J.S.); bmh@northwestern.edu (B.M.H.).

Supporting Information Available: Calculation of dipolar interactions (eqs S1–S4); Figs S1–S6; Table S1

states contain a non-heme diferric center adjacent to a tyrosyl radical (Y•)[8,9] that initiates the reduction process. The active diferric-Y• cofactor is generated from the diferrous-Y center in a reaction with O_2 and an external reductant. This process has been studied by a number of time-resolved biophysical methods, including stopped flow spectroscopy and rapid freeze-quench (RFQ) EPR, ENDOR, Mössbauer, MCD and EXAFS spectroscopies.[10–16] A paramagnetic diiron intermediate designated **X** has been observed by all of these methods. **X** is one-electron oxidized relative to the resting diferric state of β2 and is catalytically competent to oxidize tyrosine 122 to Y122•.[17,18] RFQ Q-band ^{57}Fe ENDOR spectroscopy[19] established that the diiron center of **X** has an antiferromagnetically spin coupled Fe^{III}(S = 5/2)/Fe^{IV}(S = 2) core with an S = ½ ground state.

Efforts to assign the structure(s) of **X** have been influenced by crystallographically determined structures of β2 in the diferrous state, of the tyrosyl radical reduced diferric state, and of several β2 mutants. In the diferrous state the two irons are separated by 3.9 Å with Fe1, adjacent to the tyrosine 122 that is oxidized, being 4 coordinate and Fe2 being 5 coordinate.[20,21] In this state there are no ligands from the solvent; there are two glutamates, E115 and E238, that bridge the two iron centers in a μ-1,3 fashion. In addition, Fe1 is coordinated to H118 and D84, which also is H bonded to Y122. During the conversion to the diferric cluster,[22,23] the iron centers move closer together (3.3 Å), E115 forms a single carboxylate bridge in a μ-1,3 fashion, and a single μ-oxo bridge is formed from O_2. Both iron ions become 6 coordinate. Fe1 also is coordinated to H118, bidentate to D84, and to a water or hydroxide, whereas Fe2 is coordinated to H241, monodentate to E238 and E204 and a terminal solvent molecule. Thus during the formation of active cofactor from the diferrous state, two terminal (H_xO) and μ-O have been incorporated.

The intermediate **X** formed in Y122F-β2 has been the focus of many studies because it accumulates to high levels, minimizing interference from other diiron species.[24] Studies of many other diiron proteins in different oxidation states indicate that the observed antiferromagnetic exchange-coupling between the Fe ions of **X** requires the presence of one or more oxo and/or hydroxo bridges. We previously used a combination of ^{1}H and ^{2}H CW and pulsed-ENDOR protocols to identify the types of protonated oxygen (OH_x) species and their disposition relative to the ferric and ferryl ions of **X**.[12,25] We considered the possible presence, either separately or jointly, of an hydroxo bridge, which we denoted **B**, and a terminal aqua ligand (OH_x) bound to Fe^{III}, denoted $\mathbf{T_x}$ (Fig 1). Analysis of this data led us to conclude that the inorganic core of **X** contains such a terminal aqua ligand (OH_x) but not an hydroxo bridge. In addition, the data gave no evidence for an additional H_xO terminally bound to Fe^{IV}, but did not rule it out. A subsequent ^{17}O ENDOR study of **X** prepared, either with $H_2{}^{17}O$ or with $^{17}O_2$ then led us to conclude that the [(H_xO)$Fe^{III}OFe^{IV}$] fragment in fact is the complete inorganic core of **X**.[14] This interpretation has been questioned in several recent reports, but these reports do not themselves agree on the core of **X**. The Solomon group used RFQ magnetic circular dichroism (MCD) measurements and TD-DFT calculations to propose that the core of **X** has a μ-oxo/μ-hydroxo Fe^{III}/Fe^{IV} core, but did not address the existence of terminal (H_xO) (denoted MCLBS in Fig 2).[10] In a more extensive series of computational studies, Noodleman and coworkers[26,27] instead concluded that **X** possesses a di-μ–oxo Fe^{III}/Fe^{IV} core plus a terminal (H_2O) bound to Fe^{III} ($\mathbf{T_2}$, denoted HLLN, in Fig 2).[27]

In this report we take advantage of improvements in 35 GHz pulsed-ENDOR performance to reexamine the protonation state of the oxygenic ligands of the inorganic core of **X** by *directly* probing the exchangeable proton(s) with ^{2}H pulsed-ENDOR spectroscopy. We further use ^{2}H and ^{14}N ENDOR measurements to test whether the core structure of **X** in the WT and Y122F-β2 variants are identical.

Materials and Methods

Samples

X in WT and Y122F β2 D_2O buffer was prepared by RFQ methods in[12] and stored in liquid nitrogen since 1996. 35 GHz EPR and ENDOR spectroscopy demonstrates that the signals are unchanged by this storage. The times points examined were 33 ms for **X** generated with WT-β2 and 610 or 1200 ms for Y122F-β2. In both cases, the amount of **X** is maximized at these times. A comparison of the results for the two variants thus provides insight into the role of the phenolic hydroxyl group of Y122 on the properties of **X**.

ENDOR Spectroscopy

Previous studies of **X** employed 35 GHz CW and pulsed ^{1},^{2}H ENDOR spectroscopy of exchangeable hydrogenic species associated with **X**; in this report we discuss only pulsed ^{2}H measurements. The recent upgrade to the 35 GHz pulsed-ENDOR spectrometer[28] employed in this study has been described.[29] In the text we present only ^{2}H ENDOR spectra that were collected by the Davies (t_p-T-$t_{p/2}$-τ-t_p-τ-echo) ENDOR sequence (RF applied during interval, T); in Supplementary Material we present both Davies and Mims (t_p-τ-t_p-T-t_p-τ-echo)[30] pulsed-ENDOR measurements. In all measurements, frequency values within the radio-frequency range chosen for the spectrum were accessed randomly (stochastic ENDOR). Signal averaging was accomplished by collecting multiples of such spectra, rather than by multiple acquisitions at each frequency within a spectrum.[31] The enhanced signal/noise ratio (S/N) provided by this ‘single-point stochastic ENDOR’ approach has enabled the reassessment described herein.

The enhanced S/N had one unanticipated consequence. While samples prepared in H_2O buffer previously had flat backgrounds in the ^{2}H ENDOR region, they now reveal broad features associated with ^{14}N that persist in the ^{2}H spectra for enzyme in D_2O. These features reproduce *precisely*, so many of the ^{2}H ENDOR spectra presented here have had the background subtracted, as noted in figure legends. To demonstrate that this procedure is *totally benign*, we present the corresponding primary data, foreground and background together, in Supplementary Material (Fig S1).

The Davies sequence intrinsically introduces a modulation of the ENDOR intensity that varies with the hyperfine coupling, A, and must be accounted for in simulations. The Davies ENDOR response, R, is jointly dependent on the hyperfine coupling, A, and the length of the microwave pulse, t_p, through the selectivity factor, η:

$$R=R_0\left(\frac{1.4\eta}{0.7^2+\eta^2}\right) \quad \eta=At_p \tag{1}$$

where R_0 is the maximum ENDOR response.[30] For fixed t_p, this function suppresses the ENDOR response as $A \rightarrow 0$, it rises to a maximum at $At_p = 0.7$, and then falls to zero. As a result, the ^{2}H ENDOR spectra of **X** displayed here do not show features from the weakly-coupled exchangeable protons. The Mims response shows periodic maxima and minima as function of $\eta' = A\tau$, with the first maximum at, $\eta' = 0.5$.

A deuteron ENDOR signal for a single molecular orientation consists of a doublet centered at the Larmor frequency, ν_D, and split by the orientation-dependent hyperfine coupling A; spectra in this paper are plotted as $\Delta\nu = \nu - \nu_D$. In this report, a ^{2}H ENDOR signal consists of a doublet centered at ν_D and split by A_D; the additional splitting from the nuclear quadrupole interaction expected for the (I = 1) ^{2}H nucleus is not resolved for the strongly-coupled deuteron signals discussed here. The Larmor frequency and hyperfine constants of protons and deuterons are

related by the equation: $\nu_H/\nu_D = A_H/A_D = g_H/g_D = 6.5$. As discussed in detail,[32–34] for a frozen solution sample, the determination of the full hyperfine tensor (and quadrupole tensor) of an interacting nucleus is achieved by obtaining a 2-D set of orientation-selective ENDOR spectra collected at multiple fields across the EPR envelope and comparing this set with simulated 2-D patterns. The ENDOR simulations were performed with the program Gensim, an enhanced version of the simulation program GENDOR.[32] The Davies and Mims response factors have a major influence on the observed ENDOR response, and are incorporated into Gensim.

1,^{2}H Hyperfine Interactions of protonated oxygenic ligands

Our work[12,35] has shown that the hyperfine tensor for a proton of a bridge or a terminal aqua (water/hydroxo) ligand is dominated by the through-space dipolar contribution, $\boldsymbol{T}$, arising from with interactions with the Fe ions of the diiron center of **X** ($\boldsymbol{A} = \boldsymbol{T} + a_{iso}\boldsymbol{U}$; $\boldsymbol{U}$ = unit matrix). Equations have been derived to calculate the observed dipolar coupling tensor for a nucleus in an arbitrary position relative to the two Fe ions of an $S = ½$ spin-coupled [Fe^{III}($S = 5/2$)-Fe^{IV}($S = 2$)] diiron center;[12] these equations are reproduced in Supplementary Material. The principal values are functions of the cluster's metrical parameters as defined in Supplementary Material; the component T_2 lies normal to the Fe(H)Fe plane and $\boldsymbol{T}/\boldsymbol{A}$ are rotated about the T_2/A_2 direction by the angle, γ, Fig 3 (eq S3), which also is determined by the structure. The isotropic coupling, a_{iso}, of such protons is small or even negligible.

For a terminal water (or hydroxide) the dipole interaction tensor ($\boldsymbol{T}$) with the liganding iron ion dominates the ^{1,2}H hyperfine interaction tensor ($\boldsymbol{A}$). It is approximately axial, $\boldsymbol{T} \sim [-½T, -½T, T]$, with the T_3 axis lying close to the Fe-H vector; $T \sim (7/3)g\beta g_n\beta_n/r_1^3$ when the ligand is bound to the ferric ion, but $T \sim (-4/3)g\beta g_n\beta_n/r_2^3$ when it is bound to the ferryl ion. In contrast, a proton of a bridging hydroxide interacts strongly with both Fe ions and it is characterized by a nearly rhombic dipolar tensor, $\boldsymbol{T} \sim [-T, 0, T]$, with the rotation of $\boldsymbol{T}$ about the A_2 direction such that A_1, A_3 do not point toward a specific atom.

A model-free determination of $\boldsymbol{A}$ through simulations of the experimental 2-D ENDOR field-frequency pattern gives the principal values of $\boldsymbol{A}$ and its orientation within the $\boldsymbol{g}$ tensor reference frame. As discussed in Supplementary Material, if the orientation of $\boldsymbol{A}$ is determined by the through-space dipolar interaction with the cluster Fe spins, $\boldsymbol{T}$, then the orientation of $\boldsymbol{A}$ in the molecular ($\boldsymbol{e}$) frame is determined (Fig 3) and through this the experimentally determined orientation of $\boldsymbol{g}$ relative to the $\boldsymbol{e}$ frame can be derived.[36]

Results and Discussion

EPR Spectra of X

The EPR spectra of X appear isotropic when collected at X-band, but at 35 GHz show moderately well-resolved features that permit determination of the g-tensor components. Most importantly here, this allows us to collect orientation-selective 2-D field-frequency patterns of ENDOR spectra taken at multiple fields across the EPR envelope; their analysis yields the hyperfine interaction tensors of coupled nuclei.

Alternative Models for the Identity of the Strongly-Coupled Exchangeable ^{1,2}H of X

Our previous studies[12,13] revealed ^{1,2}H ENDOR signals from strongly-coupled exchangeable proton(s), and considered their possible association with a terminal aqua ligand (OH_x) (Fig 1, top), an hydroxo bridge (Fig 1, middle), or both (Fig 1, bottom). To distinguish among these, we optimized simulations of a 2-D field-frequency pattern comprised of ^{1,2}H ENDOR spectra taken at multiple fields across the EPR envelope of **X** under the assumption either of the presence of a bridging hydroxyl (**B** model) or of an aqua ligand terminally bound to Fe^{III} (**T**

model), each with a net dipolar hyperfine coupling tensor, ***T***, to the spin-coupled iron ions given by eqs S1–4.

The geometric parameters that define the dipolar coupling calculations for the **B** and $\mathbf{T_x}$ models were chosen then as best was possible in the light of the EXAFS data available and in keeping with general bonding principles. These were used in conjunction with eqs S1–4 to generate 2-D patterns of ^{1,2}H ENDOR spectra that optimized the agreement with experiment by constraining the calculated spectra at g_1 and g_3 to match experiment. Although this constraint guaranteed a qualitative similarity between the predicted 2-D patterns of the **B** and **T** models, key differences between them, primarily in the spectra between g_2 and g_3, led us to the **T** model we reported. This model required the assumption that the terminal aqua ligand had two slightly different ^{2}H, reflecting the presence either of a terminal H_2O or a two-fold disordered hydroxyl.

In the present study we have the advantage of also being able to predict electron-nuclear dipolar interactions for **B** models based on recent DFT-determined structural models of the core of **X**. MCLBS reported their preferred structure, a **B** model. HLLN reported as their preferred model a $\mathbf{T_2}$ structure of **X** (Fig 2, LLN) that has a terminal H_2O but not an hydroxo bridge (for clarity, denoted $\mathbf{T_2}$). However they also reported the structure of a [$\mathbf{T_2}$+**B**] model, which has both types of proton, as represented by HLLN(2) in Inset 1. As discussed below, we employed the metrical parameters of these two structures as input in determining the principal values of ***T*** (Eqs S1–4) for both types of proton; these are presented in Table 1. In addition, when the two types of proton are assumed to be present simultaneously, use of the HLLN(2) structure allowed us to determine the orientation of ***g*** in the molecular (***e***) coordinate frame **(**Fig 3). We emphasize, however, that direct calculation with eqs S1–4 shows that reasonable variations to the structure of the inorganic core of **X** gives comparable results.

Deuteron ENDOR of Intermediate X

Our previous study described the basic features of the ^{1,2}H ENDOR response of **X**. It exhibits strongly-coupled, exchangeable ^{1,2}H signals, $8 \leq A(^1\text{H}) \leq 20$ MHz, from protonated oxygenic ligands, plus numerous signals from more weakly-coupled ^{1,2}H, $A(^1\text{H}) \leq 8$ MHz, some of which were exchangeable. In the study of the strongly-coupled ^{1,2}H, limitations in S/N compelled us to combine ^{1,2}H CW and pulsed measurements of **X** to obtain the 2-D field-frequency ^{1,2}H ENDOR patterns for the protonated oxygenic ligands that are used to derive hyperfine tensors. With the improved S/N now available from the pulsed spectrometer we have collected full 2-D Davies pulsed ^{2}H ENDOR patterns for these exchangeable deuteron(s) for **X** quenched in D_2O buffer.

Experiments were performed on samples of **X**(WT) (Figs 4, 5, **S1**) and **X**(Y122F) (Fig S2B, S3) freeze-quenched so that the time delays after mixing are long compared to the half-time for formation of **X**. The ^{2}H ENDOR response appears in an rf region that contains signals from ^{14}N of histidine bound to the Fe ions. To enhance the ability to compare the **^{2}H** ENDOR experiment and simulation, the spectra of **X**(WT) in Fig 4A have had the corresponding background, collected from a sample prepared in H_2O buffer, digitally subtracted. As can be seen in Fig S1 the ^{14}N features are faithfully reproduced in foreground and background spectra, and the subtraction procedure introduces no distortions. Fig S2A shows that the 2-D ^{2}H ENDOR patterns of X(WT) and **X**(Y122F) are indistinguishable, indicating that neither the mutation nor the quench delay influences this property of **X**.

Terminal ($\mathbf{T_x}$) vs Bridging (B) OH—Model-free simulation of the 2-D ^{2}H ENDOR patterns for **X** in D_2O yielded spectra that reproduce experiment with superb fidelity, Fig 4A. These simulations employed only a single (type of) contributing deuteron whose hyperfine tensor, $\boldsymbol{A_T^{ex}}$ (Table 1), has the axial character predicted for the **T** model of a terminal aqua ligand (Fig 1, **top**). The overall description matches rather well with that reported previously. However,

the superb fit to the improved data of a model with a single type of terminal deuteron now implies that if this signal represents two deuterons they must be very nearly magnetically equivalent. The principal values of the experimental dipolar interaction tensor, $\boldsymbol{T_T^{ex}}$, match well with those calculated with the dipolar equations (eqs S1–4) for a terminal [H_xO-Fe^{III}] of the **X** diiron center. The optimized location of ^{2}H relative to the iron ions ($\beta 1$, $r1$) (Table 1, **S1**) is roughly bracketed by those of the two protons of the terminal H_2O of **HLLN2 (**Fig 6, Table S1). However, note that a D_2O with this orientation would give an ENDOR pattern in which the signals from the two deuterons are resolved, contrary to experiment.

To test whether the experiments could be comparably well-described by the **B** model, we generated an optimized ^{2}H hyperfine tensor, $\boldsymbol{A_B^o}$ (Table 1), for the hydroxo bridge, as follows. We used eqs S1–4 to calculate $\boldsymbol{T_B}$ for the bridging hydroxyl of the MCLBS and **HLLN2** structures and performed simulations as the orientation of each was varied with respect to $\boldsymbol{g}$. The best results were obtained when $\boldsymbol{A_B^o}$ included the dipolar interaction similar to that of the MCLBS hydroxyl plus a small isotropic component (Table 1). These optimized simulations are overlaid on experiment in Fig 4B. As in our previous study, these simulations based on an optimized **B** model for the exchangeable deuteron reproduce the spectra at the edges of the EPR envelope (g_1 and g_3), but are poor at fields away from the edges, particularly at fields between g_2 and g_3, We thus confirm the previous conclusion that the observed ^{1,2}H signals cannot be described by assuming that the only protonated oxygenic ligand in the core of **X** is an hydroxo bridge.

As the superb simulations of the pulse ^{2}H ENDOR data in Fig 4A involve a single type of ^{2}H associated with a terminal aqua ligand, they are most simply assigned to a terminal hydroxyl with a single *major* (tier 1) orientation. The requirement of systematic variations of the ENDOR linewidth further suggests a modest distribution in position of the deuteron (tier 2 substates). However, we cannot exclude the possibility of a H_2O ligand whose two protons accidentally are equivalent and indistinguishable within the resolution of our spectra, although this seems less likely to us. The recent DFT study of HLLN inferred the presence of a water ligand to Fe^{III}, while the study of MCLBS does not address the issue.

[$\mathbf{T_x}$+B], Terminal Plus Bridging?—Could **X**, however, contain *both* **T** and **B** protons, the **[$\mathbf{T_x}$+B** model of Fig 1, as might be inferred from the MCLBS study? In our earlier study we had in fact considered this question by looking for ^{1,2}H ENDOR intensity that is not accounted for by the **T** model. A comparison of simulations for the **T** and **B** models (Fig 1) suggested that the optimal fields to look for intensity from a **B** deuteron would be in the field range from ~ g_2–g_3, where the **T** deuteron(s) had their smallest splitting and calculated **B** spectra were appreciably broader. Although we recognized that the broader signals from a **B** deuteron would presumably be less intense than the narrower signals from the **T** deuteron(s), no additional signals were detected in spectra where extensive signal averaging had produced good signal/noise ratios. We thus concluded that there is no hydroxo bridge.

The improved data reported here has allowed us to reexamine this possibility, and in doing so we have adopted a more ‘directed’ approach. In the previous study we were forced to look for signals from a **B** deuteron without knowing what fields and frequencies were best to find them, or how intense they might be if present. The present study removes this limitation. We have used multiple approaches to calculate the spectra to be expected if both **T** and **B** deuterons were present and have compared them with experiment.

To predict the ENDOR response for a hypothetical **X** with both **T** and **B** deuterons (**[$\mathbf{T_x}$+B]**, Fig 1) we assumed the presence of either one or two **T** deuterons described by $\boldsymbol{A_T^{ex}}$ (Table 1), namely either a terminal hydroxo ($\mathbf{T_1}$) or a terminal water ($\mathbf{T_2}$ in Fig 2) that has two magnetically equivalent deuterons. As the most straightforward approach to describing a **B**

deuteron, we assigned to **B** the hyperfine tensor $\boldsymbol{A_B^0}$, as defined above (Table 1), and calculated the 2-D field-frequency patterns expected if both **T** and **B** deuterons were present, Fig 4C. To ensure that we have given the best chance for this model to succeed, we minimized the predicted detectability of **B** by employing for the **T** deuteron the field-dependent linewidth used in Fig 4A, while using for **B** a linewidth at all fields that equaled the largest linewidth found for the **T** deuteron(s) at any field (the value near g_1), rather than the optimized linewidth for each field as used in Fig 4B. Fig 4C displays the resulting composite 2-D ^{2}H ENDOR pattern calculated for models with both x = 1 and x = 2 protons on the terminal OH_X, along with the **B** deuteron, [$\mathbf{T_1}$+**B**] and [$\mathbf{T_2}$+**B**] models respectively, each overlaid onto the experimental ^{2}H ENDOR pattern for **X**(WT); Fig 5 separately presents the experimental and calculated spectra for fields at which the presence of a **B** deuteron would be most obvious. In fact, it is obvious that *none* of the intensity predicted for a **B** deuteron is present in the experimental spectra.

As an alternate means of simulating the **[$\mathbf{T_1}$ (or) $\mathbf{T_2}$ +B]** model of **X** we employed the **HLLN2** structure for **X** (Fig 6) in a recently developed simulation approach.[36] As shown in the figures, **HLLN2** incorporates a H_2O terminally bound to Fe^{III}, an hydroxo bridge that carries the **B** proton, as well as an oxo bridge. To calculate the ^{2}H ENDOR spectra expected for this **B** proton, we assigned the experimentally determined **T**-proton hyperfine tensor, $\boldsymbol{A_T^{ex}}$, first to one of the deuterons of the terminal H_2O of **HLLN2** (eg., H_T of Fig 6) then to the other, in each case taking $\boldsymbol{A_T^{ex}}$ as coaxial with $\boldsymbol{T_T}$ calculated with eqs S1–4; then we used our the experimentally determined orientation of $\boldsymbol{A_T^{ex}}$ relative to $\boldsymbol{g}$ to fix the orientation of $\boldsymbol{g}$ in the molecular frame (Fig 6). Once this was known, we could use eqs S1–4 to calculate the dipolar interaction for the **B** deuteron, $\boldsymbol{T_B}$, from the HLLN(2) structure and to compute the 2-D patterns of ^{2}H ENDOR spectra to be expected if both types of deuteron were present.

In all these computations, as shown in Figs S4, S5, the simulations predict additional ^{2}H ENDOR intensity associated with **B** that would be even more obvious and readily detected than if a bridging proton had the optimized hyperfine tensor, $\boldsymbol{A^B}$, Fig 5. *No such intensity is seen in the experiment*.

A technical observation about the experiments and simulations also is of interest. Each of the ENDOR simulations of Figs 4, 5 is a 'statistical/geometric' sum of the contributions from the subset of orientations that contributes to the EPR spectrum at the *g*-value of observation.[32] In such a simulation, the integrated ENDOR intensity of a **T** and **B** deuteron would be equal. As the **B** spectrum is broader and is calculated with a greater component ENDOR linewidth, if 'statistical/geometric' considerations were all that were important for determining intensities, the relative intensities of features associated exclusively with **B** would be much less than those of the **T** proton, making the detection of **B** harder than it is seen to be in Fig 5. However, the sharp **T** doublet has a smaller hyperfine coupling and is suppressed to a greater degree by the Davies ENDOR response (eq 1). Thus, curiously, while the suppression effect reduces the overall S/N of the spectra, it helps enable us to state with confidence that **X** does not contain a **B** proton in addition to the **T** proton(s).

In short, the absence in the spectra of <u>any</u> of the unexplained features that would be <u>required</u> for the proton of a μ–OH) bridge rules out the presence of such a moiety, either alone or in addition to the Fe^{III}-bound terminal aqua ligand (H_xO): only the latter is present ($\mathbf{T_X}$ *model of*Fig 1), *in agreement with our proposal of over a decade ago.*[12]

The model for the inorganic core of **X** favored by HLLN agrees with our earlier proposal and current conclusion regarding the protonation state of the **X** core (Fig 2), whereas the recent MCD measurements of MCLBS instead were interpreted to favor an hydroxo bridge. A critical comparison of the two methods is thus in order. *Firstly*, the present ENDOR measurements *directly* interrogate the protonated oxygenic ligands of **X**, whereas optical methods only

indirectly infer the sites of protonation. Furthermore, ENDOR is insensitive to diamagnetic forms of RNR that may be present in sample preparations, whereas the optical methods include signals from all states of RNR. *Secondly*, the electronic structure assignments of MCLBS and the corresponding assignment of a μ-hydroxo bridge derive from their assignment of all three d-d transitions to the d-π manifold of **X**, based in part on the conclusion that the splittings are too large to be associated with a bis-μ-oxo structure. The more extensive computations of HLLN, associated with a more realistic model of protein ligands to the diiron center, lead them to assign the optical bands differently, thereby leading them to reject the HLLN structure that has no μ-hydroxo bridge, Fig 2. *Lastly*, for completeness, we suggest that a more rigorous test of the new sample preparation procedure of MCLBS, which differ from that used in all previous RFQ studies[12–15,19,37,38] would be welcome. The MCD study involved freeze-quenching by spraying into liquid nitrogen, rather than liquid pentane, which gives longer freezing times. Also, high concentrations of glycerol were added at −30°C as a glassing agent subsequent to freeze-quenching. Although MCLBS carried out 9 GHz EPR experiments to test whether X prepared in their procedure is the same as in the samples prepared previously, the signal of X appears isotropic at X band and is not a particularly sensitive test for subtle structural differences that might occur.

Other ^{1,2}H ENDOR signals and the possibility of a H_xO bound to Fe^{IV}

In our earlier work we observed non-exchangeable ^{1}H ENDOR signals from the protein matrix, to be associated with ligands to the diiron center and nearby amino acids. In addition, we saw weakly-coupled exchangeable ^{2}H signals, presumably from histidine-imidazole, amino/amido N-H, etc. We found no evidence for exchangeable ^{2}H ENDOR signals that would be associated with a H_xO bound to Fe^{IV}. Combining this with the subsequent failure to find a ^{17}O signal from such a species, we concluded that none was present. In the present study we also reconsidered the possibility of a H_xO bound to Fe^{IV}. Such a proton is predicted (eqs S1–4) to have a roughly rhombic dipolar tensor with maximum ^{2}H tensor components of ~ 2 MHz. To test for signals from such a proton we collected both ^{2}H Mims (Fig S6) and ^{2}H 'soft (t_p = 200 ns)' Davies pulsed- ENDOR spectra (Figs 4, S1) but neither gave any evidence for ^{1,2}H ENDOR intensity for such a proton. Thus, the present effort is consistent with our earlier conclusion, as well as with the computations of HLLN.

Possible Effects of the Y122F Mutation

The 2-D patterns of ^{2}H ENDOR spectra of **X**(WT) and **X**(Y122F) are identical, within error (Fig S2A), as are the hyperfine tensors determined by simulating those patterns (Table 1; Figs 4A and S2B). To search for other possible influences of the mutation we collected 2-D field-frequency plots of ^{14}N ENDOR spectra for **X**(WT) and **X**(Y122F). Fig S3 shows that these plots for the two likewise are indistinguishable.

Conclusions

In this report we take advantage of improvements in 35 GHz pulsed ENDOR signal/noise to reexamine the protonation state of the oxygenic ligands of inorganic core of **X** directly by probing the exchangeable protons of **X**(WT) and **X**(Y122F) with ^{2}H pulsed-ENDOR spectroscopy. The 2-D pattern of Q-band ^{2}H ENDOR spectra collected for the strongly-coupled exchangeable proton(s) of **X**(WT and Y122F) are indistinguishable (Fig S2A), and the same is true for ^{14}N ENDOR measurements of histidyl ligands bound to Fe, together indicating that the Y122F mutation does not alter the properties of **X**.

Simulations of the ^{2}H 2D-field-frequency ENDOR patterns, Figs 4A, S2B, of **X** show that the exchangeable proton/deuteron signals belong to the proton of a terminal aqua ligand bound to Fe^{III} (Fig 1, $\mathbf{T_X}$-model), likely an hydroxo ligand. Simulations based on both the **B** and

[T_X+B] models (Figs 4B, 4C, S4 and S5) completely fail to reproduce the data, demonstrating that **X** does *not* contain an hydroxo bridge, either alone **(B)** or with a terminal aqua ligand **[T_X+B]**. The measurements further support the conclusion that there is no aqua ligand bound to Fe^{IV}. Overall, these findings thus establish that the inorganic core of **X** does not include a μ-hydroxo bridge, and does contain the [$(H_xO)Fe^{III}OFe^{IV}$] fragment that defines the **T_X**-model (Fig 1; top). We shall next use the enhanced 35 GHz pulsed-ENDOR capabilities to revisit the question of whether **X** contains the second oxo bridge of a diamond core, as favored by both HLLN and MCLBS, by exploring the fate of the two atoms of dioxygen and the incorporation of solvent O through *direct* interrogation of those atoms by ^{17}O ENDOR spectroscopy.

Supplementary Material

Refer to Web version on PubMed Central for supplementary material.

Acknowledgments

The authors would like to express their gratitude towards C. E. Davoust for his technical support and to the NIH (Grants HL 13531 (B. M. H); GM 29595 (J. S.)).

References

1. Eklund H, Uhlin U, Farnegardh M, Logan D, Nordlund P. Progress in Biophysics & Molecular Biology 2001;77:177–268. [PubMed: 11796141]
2. Solomon EI, Brunold TC, Davis MI, Kemsley JN, Lee SK, Lehnert N, Neese F, Skulan AJ, Yang YS, Zhou J. Chem Rev (Washington, DC, U S) 2000;100:235–349.
3. Nordlund P, Eklund H. Curr Opin Struct Biol 1995;5:758–766. [PubMed: 8749363]
4. Feig AL, Lippard SJ. Chem Rev (Washington, DC, U S) 1994;94:759–805.
5. Licht, S.; Stubbe, J. Mechanistic investigations of ribonucleotide reductases; Comprehensive Natural Product Chemistry. Poulter, C Dale, editor. Vol. 5. Elsevier Science; New York: 1999. p. 163-203.
6. Stubbe J, Riggs-Gelasco P. Trends Biochem Sci 1998;23:438–443. [PubMed: 9852763]
7. Stubbe J, van der Donk WA. Chem Rev (Washington, DC, U S) 1998;98:705–762.
8. Atkin CL, Thelander L, Reichard P, Lang G. J Biol Chem 1973;248:7464–7472. [PubMed: 4355582]
9. Larsson A, Sjöeberg BM. EMBO J 1986;5:2037–2040. [PubMed: 3019680]
10. Mitic N, Clay MD, Saleh L, Bollinger JM, Solomon EI. J Am Chem Soc 2007;129:9049–9065. [PubMed: 17602477]
11. Riggs-Gelasco PJ, Shu L, Chen S, Burdi D, Huynh BH, Que L Jr, Stubbe J. J Am Chem Soc 1998;120:849–860.
12. Willems JP, Lee HI, Burdi D, Doan PE, Stubbe J, Hoffman BM. J Am Chem Soc 1997;119:9816–9824.
13. Burdi D, Sturgeon BE, Tong WH, Stubbe J, Hoffman BM. J Am Chem Soc 1996;118:281–282.
14. Burdi D, Willems J, Riggs-Gelasco P, Antholine W, Stubbe J, Hoffman B. J Am Chem Soc 1998;120:12910–12919.
15. Ravi N, Bollinger JM Jr, Huynh BH, Edmondson DE, Stubbe J. J Am Chem Soc 1994;116:8007–8014.
16. Bollinger JM Jr, Tong WH, Ravi N, Huynh BH, Edmondson DE, Stubbe J. J Am Chem Soc 1994;116:8024–8032.
17. Bollinger JM Jr, Edmondson DE, Huynh BH, Filley J, Norton JR, Stubbe J. Science 1991;253:292–298. [PubMed: 1650033]
18. Bollinger JM Jr, Tong WH, Ravi N, Huynh BH, Edmondson DE, Stubbe J. J Am Chem Soc 1994;116:8015–8023.
19. Sturgeon BE, Burdi D, Chen S, Huynh BH, Edmondson DE, Stubbe J, Hoffman BM. J Am Chem Soc 1996;118:7551–7557.

20. Logan DT, Su XD, Aberg A, Regnstrom K, Hajdu J, Eklund H, Nordlund P. Structure 1996;4:1053–1064. [PubMed: 8805591]
21. Wei, P-p; Skulan, AJ.; Mitic, N.; Yang, Y-S.; Saleh, L.; Bollinger, JM., Jr; Solomon, EI. J Am Chem Soc 2004;126:3777–3788. [PubMed: 15038731]
22. Nordlund P, Eklund H. J Mol Biol 1993;232:123–164. [PubMed: 8331655]
23. Nordlund P, Aberg A, Eklund H. Biochemistry Soc Trans 1993;21:735–738.
24. Tong W, Burdi D, Riggs-Gelasco P, Chen S, Edmondson D, Huynh BH, Stubbe J, Han S, Arvai A, Tainer J. Biochemistry 1998;37:5840–5848. [PubMed: 9558317]
25. Willems, J-P.; Lee, H-I.; Burdi, D.; Doan, PE.; Stubbe, J.; Hoffman, BM. ACS Advances in Chemistry. Solomon, E.; Hodgson, K., editors. American Chemical Society; Washington D.C: 1998. p. 2-15.
26. Han WG, Liu T, Lovell T, Noodleman L. Inorg Chem (Washington, DC, U S) 2006;45:8533–8542.
27. Han WG, Liu T, Lovell T, Noodleman L. J Am Chem Soc 2005;127:15778–15790. [PubMed: 16277521]
28. Davoust CE, Doan PE, Hoffman BM. J Magn Reson 1996;119:38–44.
29. Zipse H, Artin E, Wnuk S, Lohman GJS, Martino D, Griffin RG, Kacprzak S, Kaupp M, Hoffman B, Bennati M, Stubbe J, Lees N. J Am Chem Soc. 2008In Press
30. Fan C, Doan PE, Davoust CE, Hoffman BM. J Magn Res 1992;98:62–72.
31. Epel B, Arieli D, Baute D, Goldfarb D. J Magn Reson 2003;164:78–83. [PubMed: 12932459]
32. Hoffman BM, DeRose VJ, Doan PE, Gurbiel RJ, Houseman ALP, Telser J. Biol Magn Reson 1993;13 (EMR of Paramagnetic Molecules):151–218.
33. Hoffman BM. Acc Chem Res 2003;36:522–529. [PubMed: 12859213]
34. Hoffman B. Proc Natl Acad Sci U S A 2003;100:3575–3578. [PubMed: 12642664]
35. DeRose VJ, Liu KE, Lippard SJ, Hoffman BM. J Am Chem Soc 1996;118:121–134.
36. Lees NS, McNaughton RL, Gregory WV, Vela J, Holland PL, Hoffman BM. J Am Chem Soc 2008;130:546–555. [PubMed: 18092774]
37. van der Donk WA, Stubbe J, Gerfen GJ, Bellew BF, Griffin RG. J Am Chem Soc 1995;117:8908–8916.
38. Bollinger, JM., Jr; Tong, WH.; Ravi, N.; Huynh, BH.; Edmondson, DE.; Stubbe, J. Methods Enzymol. Klinman, JP., editor. Academic Press; New York: 1995. p. 258
39. Additional solutions are closely related and need not be considered separately

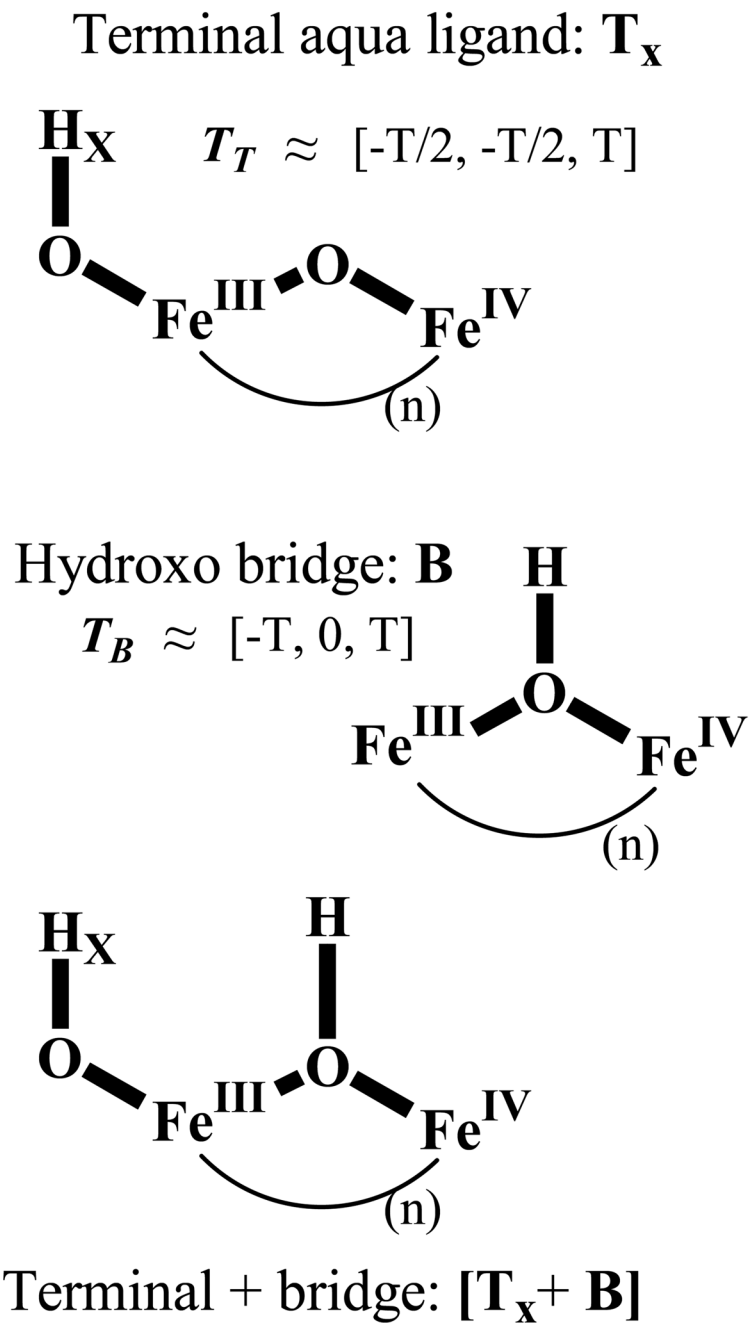

Fig 1.

Alternate, models for exogenous ligands to **X**, with the portions relevant to this study in bold. *Top*, oxo bridge plus terminal aqua ligand (**$\mathbf{T_X}$**); *middle*, hydroxo bridge (**B**); *bottom*, terminal aqua plus bridge [**$\mathbf{T_X}$+B]**. Approximate characteristics of the ^{1,2}H cluster dipolar hyperfine tensors are indicated (eqs S1–4).

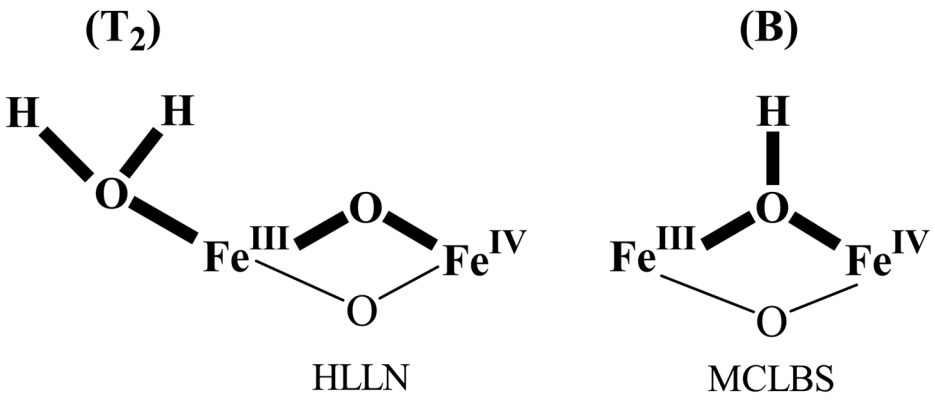

Fig 2.

Inorganic cores of **X** models proposed by Noodleman and coworkers (HLLN)[27] and by Solomon and coworkers (MCLBS),[10] with the portions relevant to this study in bold.

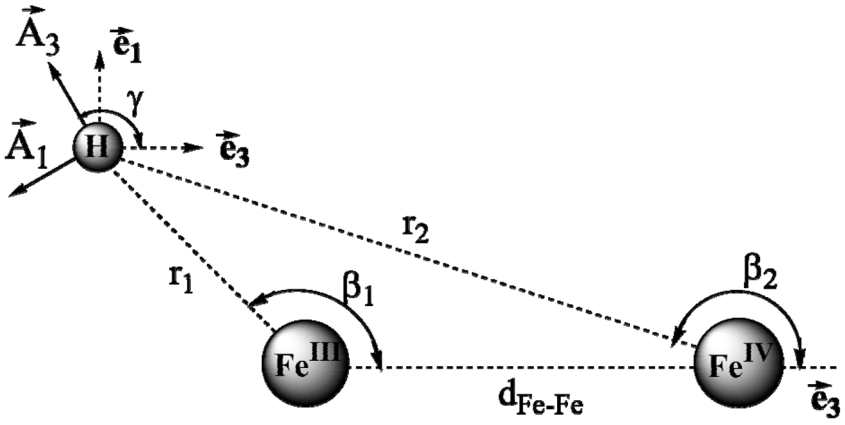

Fig 3.
Geometry used in calculation of cluster dipolar interaction tensor, ***T*** (eqs S1–4).

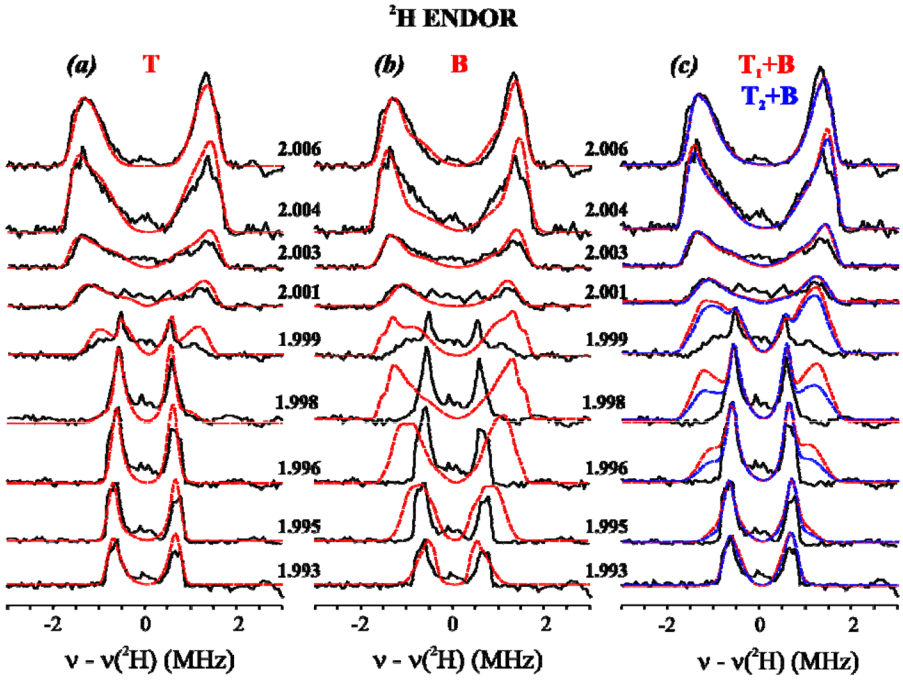

Fig 4.

Experimental 2-D field-frequency plots of Davies ^{2}H ENDOR spectra **of X**(WT) in D_2O. Red and blue curves are simulations with the three models considered here (Fig 1; see text and Table 1): ***(a)*** **T**; ***(b)*** **B**, ***(c)*** [$\mathbf{T_X}$**+B]**, considered here. *Conditions:* π-pulse length = 200 ns, τ = 600 ns, repetition time = 50 ms, MW frequency = 34.826 GHz, T = 2 K. All spectra are centered at the ^{2}H nuclear Larmor frequency. Backgrounds have been subtracted from experimental spectra as discussed (See Materials and Methods and Supplementary Materials.).

(a) Experiment with **T** proton simulations overlaid. Simulation parameters (determined as described in text): $\boldsymbol{g}$ = [g_1 = 2.0056, g_2 = 1.9977, g_3 = 1.993], $\boldsymbol{A}$ = [A_1 = −1.55, A_2 = −1.15, A_3 = 3.2] MHz (Euler angles α = 10.5°, β = 72°, γ = 0), line widths used = 0.09 (minimum) to 0.25 (maximum) MHz.

(b) Experiment with simulations of the **B** proton model, optimized by including a_{iso}. Spin Hamiltonian parameters for the bridging hydroxide (optimized); $\boldsymbol{g}$ = [g_1 = 2.0056, g_2 = 1.9977, g_3 = 1.993], $\boldsymbol{A}$ = [A_1 = −3.031, A_2 = −0.948, A_3 = 3.179] MHz (Euler angles α = 0.0°, β = 115.0°, γ = 75.0°), linewidths range from 0.08 (minimum) to 0.25 (maximum) MHz.

(c) Experiment with simulations of [$\mathbf{T_X}$**+B**] models: *x = 1* (red), *x = 2* (blue). Parameters for the simulations of terminal and the optimized bridging hydroxides: see F**igs 4A**, **4B** and Table 1. For x = 1, the intensities of the **T** and **B** deuteron signals were added and the resultant scaled to the maximum of the experiment; for x = 2, twice the **T** intensity was added to the **B** intensity before scaling.

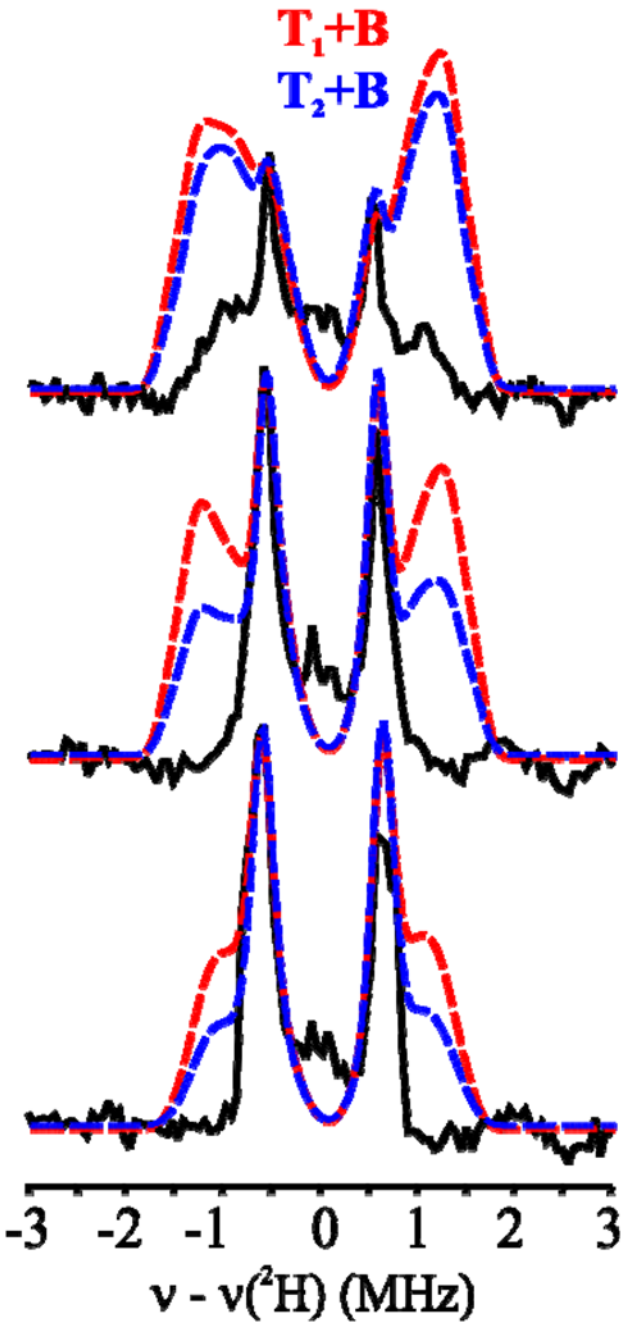

Fig 5.
Decisive comparisons between experimental ^{2}H-ENDOR responses for **X**(WT) and simulations for the [$\mathbf{T_X}$+**B**] models, as described in Fig 4: g = 1.999, 1.998 and 1.996.

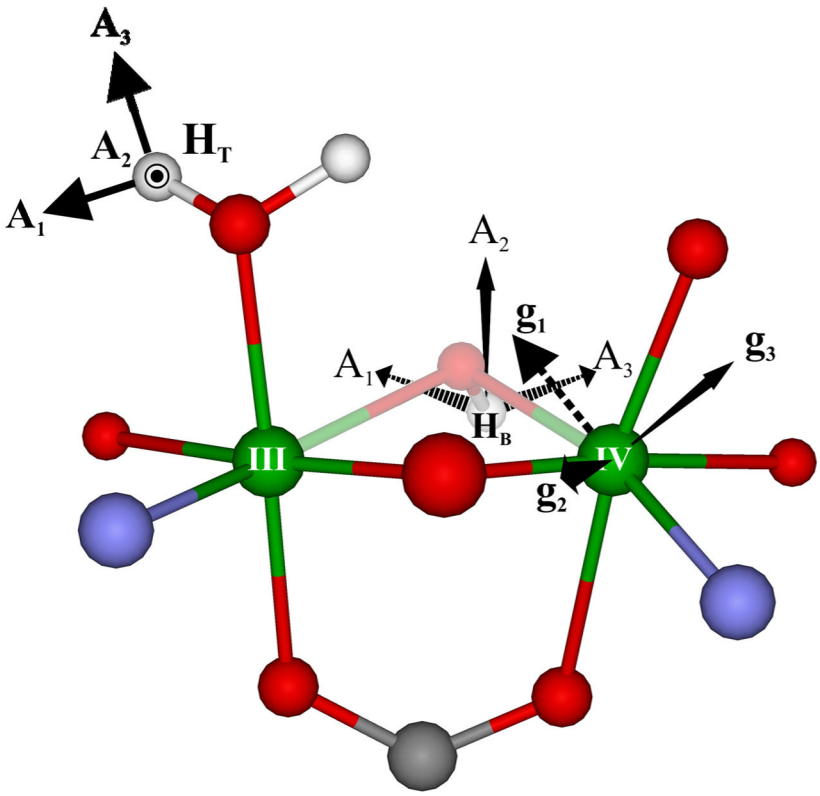

Fig 6.

Orientation of $\boldsymbol{A_T}$, $\boldsymbol{T_B/A_B}$ for H^T of the hypothetical HLLN(2) model of **X**, along with the orientation of $\boldsymbol{g}$ in the molecular frame as determined from $\boldsymbol{A_T}$ and experimental simulation parameters (See Supp. Mat). $\boldsymbol{T_T}$ is not shown for the other terminal proton.

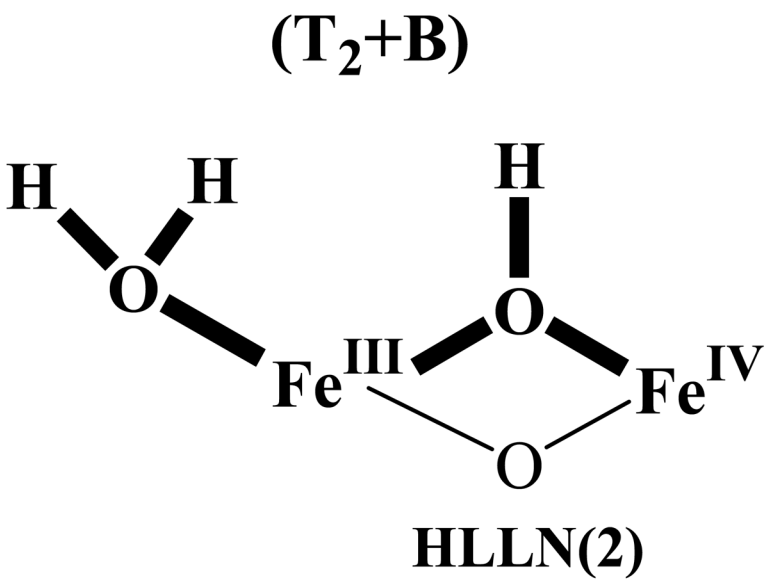

Inset 1.

Table 1

Metrical and ^{2}H spin Hamiltonian parameters used to calculate[a] the 2-D ENDOR patterns displayed in Figs. 4A and 4B

	Terminal OH_X–			Bridging OH^-		
	Experimental		Calculated[c]	Optimized		Calculated[d]
	($\boldsymbol{A^{ex}}$)[b]	($\boldsymbol{T^{ex}}$)	(***TT***)	($\boldsymbol{AB^0}$)[b]	($\boldsymbol{TB^0}$)	(***TB***)
A1/*T1*(MHz)	−1.55	−1.717	−1.718	−3.031	−2.764	−2.762
A2/*T2*(MHz)	−1.15	−1.317	−1.316	−0.948	−0.681	−0.681
A3/*T3*(MHz)	3.2	3.033	3.034	3.179	3.446	3.443
λ		0.132	0.132		0.604	0.604
Aiso(MHz)	0.167			−0.267		
r1(Å)[e]			2.625			2.67
β (°)			94.5			59.3
γ (°)			90.0			50.1
d_{FeFe}(Å)			2.84			2.817

[a] Simulations employed $g = [g_1, g_2, g_3] = [2.0056, 1.9977, 1.993]$. Quadrupole splitting for ^{2}H (I = 1) are not resolved, their inclusion had no effect on simulations, so were not incorporated.

[b] The Euler angles for $\boldsymbol{A^{ex}}$ are $\alpha = 10.5°$, $\beta = 72.0°$ and $\gamma = 0.0°$. The Euler angles for $\boldsymbol{A^B}$ $\alpha = 0.0°$, $\beta = 115.0°$ and $\gamma = 75.0°$. For definition of angles, see Ref32.

[c] Best match between $\boldsymbol{T^{ex}}$ and **T** as calculated by eqs S1–4.

[d] Calculated by slight optimization of the HLLN(2) structure.

[e] r_1, β, γ and d_{FeFe} are defined in Fig 3.

J Am Chem Soc. Author manuscript; available in PMC 2010 March 11.